PHYSICAL REVIEW E **73**, 031302 (2006)

Continuum approach to wide shear zones in quasistatic granular matter

Martin Depken and Wim van Saarloos
Instituut-Lorentz for Theoretical Physics, Leiden University, P.O. Box 9506, NL-2300 RA Leiden, The Netherlands

Martin van Hecke
Kamerlingh Onnes Lab, Leiden University, P.O. Box 9504, 2300 RA Leiden, The Netherlands

(Received 1 November 2005; published 7 March 2006)

Slow and dense granular flows often exhibit narrow shear bands, making them ill suited for a continuum description. However, smooth granular flows have been shown to occur in specific geometries such as linear shear in the absence of gravity, slow inclined plane flows and, recently, flows in split-bottom Couette geometries. The wide shear regions in these systems should be amenable to a continuum description, and the theoretical challenge lies in finding constitutive relations between the internal stresses and the flow field. We propose a set of testable constitutive assumptions, including rate independence, and investigate the additional restrictions on the constitutive relations imposed by the flow geometries. The wide shear layers in the highly symmetric linear shear and inclined plane flows are consistent with the simple constitutive assumption that, in analogy with solid friction, the effective-friction coefficient (ratio between shear and normal stresses) is a constant. However, this standard picture of granular flows is shown to be inconsistent with flows in the less symmetric split-bottom geometry—here the effective friction coefficient must vary throughout the shear zone, or else the shear zone localizes. We suggest that a subtle dependence of the effective-friction coefficient on the orientation of the sliding layers with respect to the bulk force is crucial for the understanding of slow granular flows.

DOI: 10.1103/PhysRevE.73.031302 PACS number(s): 45.70.Mg

I. INTRODUCTION

Granular flows show a very wide variety of behaviors, and while the microscopic dynamics of dry cohesionless grains is simple and well understood, there is no general theory describing their emergent macroscopic properties. Flowing grains can roughly be classified into three regimes by the relative importance of inertial effects [1]. For strong external driving the grains form a gaseous state. Here particle interactions are dominated by binary collisions, and this regime is well captured by modified kinetic theories [2–5]. On lowering the driving strength the flow becomes denser, with collisions becoming correlated and often involving several particles at once. In this regime inertia is still important, but kinetic theories become increasingly difficult to justify and apply [6]. On further lowering the driving strength, the granular media enter the quasi-static regime where inertial effects are negligible. The grains form enduring contacts, leading to highly complex contact and force networks. The modeling of these flows is still in its infancy, and there is no *general* approach which, for given geometry and grain properties, predicts the ensuing flow fields.

Most slow granular flows cannot be considered smooth. Their flow fields vary strongly on the grain scale. For example, in many experimental realizations one observes shear localization where the flow of the material is concentrated into a very narrow shear band [7–10]. In such situations the flow can be modeled as two solid blocks sliding past each other. If the shear stress, τ, is simply proportional to the normal pressure, P, then these materials are referred to as ideal cohesionless Coulomb materials. Many formulations of granular flow focus immediately on this narrow shear band regime [8,10].

However, there are a number of systems that display smooth velocity fields and wide shear zones. These should be amenable to a continuum description. Among these is the planar-shear cell without gravity, which has been examined numerically in Refs. [11–16] [Fig. 1(a)]. Another example is slow flow down inclined planes, which in simulations of three-dimensional (3D) systems appear to reach a quasistatic state [17] [Fig. 1(b)]. Though conceptually simple, both of these situations are hard to realize experimentally. In recent experiments, using a modified Taylor-Couette cell with split bottom [Fig. 1(c)], robust and wide shear zones were obtained in the quasistatic, dense regime [18–20]. While we do not expect there to be a "universal" continuum theory of

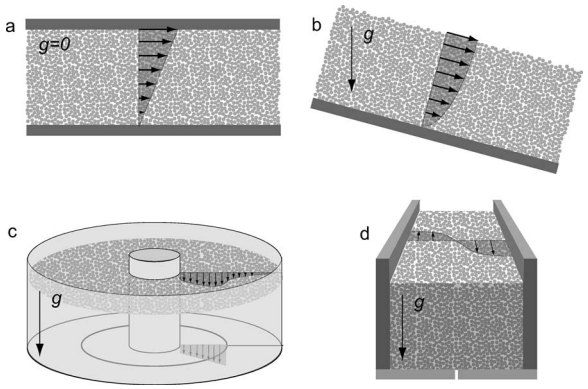

FIG. 1. Geometries in which smooth, quasistatic grain flows occur. The velocity field is sketched with arrows. (a) Linear shear in absence of gravity. (b) Inclined plane flow close to the critical inclination angle. (c) Taylor-Couette flow with split bottom. (d) Linear shear over a split bottom.

granular flow, these observations strongly suggest that there is a continuum theory with its own domain of validity, that should capture this smooth quasistatic granular flow regime.

Our approach is to test whether a straightforward continuum model of these smooth flow fields, based on a minimum of readily testable physical assumptions, can be made consistent with the numerical and experimental data available for smooth quasistatic flows. In addition to mass, linear- and angular-momentum conservation, we need to find additional relations between the six components of the stress tensor σ_{ij} and the state of the system characterized by such quantities as strain history, packing fraction, etc. Such constitutive equations are particularly simple for Newtonian fluids (leading to the Navier-Stokes equation) and elastic solids (leading to the equations of linear elasticity). The yielding behavior of granular media illustrates that the constitutive equations must here take on a more complicated form. Granular media are athermal and dissipative—hence, when no external energy is supplied, grains *jam* into a rigid, solidlike state which can sustain a finite load before yielding [21]. Grains are made to flow by supplying an external (shear) stress to overcome this yielding threshold. As a result, for very slow and dense granular flows, the shear stresses are finite and do not approach zero. This complicates matters considerably.

Our approach has two important ingredients, the details of which can be found in Sec. II. First, we are guided by the well-known fact that dense grain flows exhibit rate independence [11]. For the velocity fields this means that, to good approximation, the entire velocity profile scales identically with the external driving: When the driving speed is doubled, the whole velocity field doubles. The stresses are also approximately rate independent, meaning that when the speed is doubled, the stresses stay the same. This makes the relation between the stresses and the flow field rather special, and even if we could determine the full stress field, we could never hope to get the full velocity profile. The approach we take relates the stresses to certain aspects of the *geometry* of the flow. This results in statements regarding material sheets in the flow, within which the particles on average only perform a collective rigid body motion with respect to each other. A trivial instance of such sheets are the layers of constant velocity present in the linear setups in Figs. 1(a) and 1(b), and illustrated in Fig. 3. In order to say something about the actual velocities of such planes one would have to appeal to a subdominant dependence on shear rate.

Second, when the grains are flowing, they experience large fluctuations [22]. Hence, we assume that if in a certain plane the strain rate is zero, then there will be no residual shear stress in this plane—if there was a shear stress, there would be a shear flow. Hence, all shear stresses are dynamically sustained, and there are no elastic shear stresses. Thus, we will not attempt to model a mixture of solid and flowing behavior as done in Ref. [23]. This implies that the principal strain and stress directions are the same (see Sec. II C).

In Sec. III we apply this framework to the four geometries depicted in Fig. 1. In the linear geometries [Figs. 1(a) and 1(b)], symmetry considerations directly give that the principal directions are constant throughout the system, and thus the equations are automatically closed. This gives the standard Mohr-Coulomb relation $\tau=\mu P$, with the effective-friction coefficient necessarily constant throughout the sample. For the less symmetric geometries [Figs. 1(c) and 1(d)] the local orientation of the above material sheets will vary throughout the cell. This allows us to separate the effect of constitutive assumptions regarding the rates in the system and the geometry of the flow (see Sec. II B for further details). If we maintain that the effective friction coefficient is constant throughout the sample, we find that the shear zones have infinitesimal width. *The standard approach of a constant effective-friction coefficient between shearing planes fails* (see Sec. III B 1, and especially Fig. 6). In fact, we then completely recover the prediction regarding the location of the shear zone that was derived on the basis of torque minimization by Unger *et al.* in [24].

To capture the experimentally observed widening of the shear zone in the bulk, the effective-friction coefficient has to vary throughout the shear zone. We argue that this can only be done through a dependence of the effective-friction coefficient on the orientation of the shearing surface with respect to any bulk force (here gravity). The possible origin of such an angle dependence is discussed in Sec. IV.

II. QUASISTATIC GRANULAR FLOWS

At the heart of the present development lies the peculiar fact that in order for a granular matter to support a shearing state, no matter how slow, a finite shear stress is needed. This is reminiscent of solid friction, but in stark contrast with the situation in Newtonian fluids. This feature is clearly visible in the experimental results reported in [11,25–27].

A. Explicit rate independence

The strain-rate tensor $\underline{\underline{D}}=(\underline{\underline{\nabla v}}+(\underline{\underline{\nabla v}})^{\dagger})/2$ plays a central role in ordinary fluid mechanics [28]. The use of only the symmetric part of the deformation-rate tensor $\underline{\underline{\nabla v}}$ ensures that no stresses are induced by pure local rotations of the material (principle of material objectivity). In the theory of simple fluids one assumes that the knowledge of the complete history of $\underline{\underline{D}}$, for any material point, will give the stresses at that point. In the case that there are no memory effects this means that the stress tensor can be expressed as an isotropic tensor function of the strain rate tensor. For such functions, the first representation theorem (Rivlin-Ericksen theorem [29]) states that the most general constitutive equation can be written as

$$\underline{\underline{\sigma}} = \alpha_0 \underline{\underline{I}} + \alpha_1 \underline{\underline{D}} + \alpha_2 \underline{\underline{D}}^2, \tag{1}$$

with $\alpha_i=\alpha_i(I_D,II_D,III_D)$, and the invariants

$$I_D = \mathrm{tr}\underline{\underline{D}}, \quad II_D = \mathrm{tr}\underline{\underline{D}}^2, \quad III_D = \det \underline{\underline{D}}.$$

As mentioned above, the granular flows that we want to describe are such that we have finite shear stresses even as the shear rate approaches zero. Thus, we can split the stress tensor, $\underline{\underline{\sigma}}$, into a rate-independent part, $\underline{\underline{\sigma}}_0$, and a rate-dependent part, $\underline{\underline{\sigma}}_1$,

$$\underline{\underline{\sigma}} = \underline{\underline{\sigma}}_0 + \underline{\underline{\sigma}}_1, \tag{2}$$

in such a way that $\underline{\underline{\sigma}}_0$ is *not* proportional to the identity operator (i.e., it contains shear stresses, and is hence not simply a hydrostatic pressure), and $\underline{\underline{\sigma}}_1$ vanishes as the strain rates approaches zero. The condition on $\underline{\underline{\sigma}}_0$ directly tells us that in the zero shear rate limit α_1 and/or α_2 must be singular.

Theoretically there exist a flow regime in which $\underline{\underline{\sigma}}_0$ alone sets certain properties of the flow. We will refer to this regime as quasistatic (the precise experimental definition is given in Sec. II E). The information that can be extracted from the rate-independent part of the stress tensor will in general be of the type specifying, e.g., constant velocity surfaces. Due to rate independence, questions regarding the magnitude of the velocity field cannot be answered by considering this limit alone, and neither can questions regarding the stability of any wide shear zones.

We further assume that there are only local interactions in the bulk (principle of local action) [30]. The implicit assumption in our approach is that our continuum description is valid, upon coarse graining over some small but finite length scale.

As for the history dependence, the systems we consider are such that the flow direction is also a symmetry direction. For such system in steady shearing states, any material point will always have the same surrounding flow field. Thus $\underline{\underline{D}}$ does not change (up to a rotation) along the evolution paths of the material elements, and memory effects are washed out.

The strain-rate tensor is symmetric, and is hence completely specified by six parameters. We can choose these parameters as, e.g., the principal strain rates, and the orientation of the principal directions (specified by three angles). Using this parametrizations of the strain-rate tensor enables us to isolate the rate dependence from the orientational dependence. We denote the principal strain rates with γ_i, and the three angles defining the principal directions by θ_i. The angles are to be taken with respect to some suitably chosen local reference direction (e.g., the gravitational field). Then, the general form of the stress tensor is

$$\underline{\underline{\sigma}}_0 = \underline{\underline{\sigma}}_0(\gamma_1, \gamma_2, \gamma_3, \theta_1, \theta_2, \theta_3, \dots), \tag{3}$$

where the dots indicate a possible dependence on parameters not directly related to the shear. Rate independence of the stress tensor implies invariance under the rescaling $\underline{v} \to b\underline{v}$, and consequently invariance under $\underline{\underline{D}} \to b\underline{\underline{D}}$ ($\Leftrightarrow \gamma_i \to b\gamma_i$). Therefore the stresses can only depend on the ratios of the principal-strain rates, and not the strain rates themselves. Hence,

$$\underline{\underline{\sigma}}_0 = \underline{\underline{\sigma}}_0(\gamma_1/\gamma_3, \gamma_2/\gamma_3, \theta_1, \theta_2, \theta_3, \dots). \tag{4}$$

To proceed with a general theory one would need to include the full dependence on the principal-strain-rate ratios. The flows we will consider are of a limited type, which enables us to study the influence of the angles θ_i without specifying the dependence on the principal-strain-rate ratios. We now proceed by clarifying his point.

B. Shear-free sheets

The systems we wish to consider are all such that, on the scale of the coarse graining, one can think of them as consisting of material sheets, with no internal shear, shearing past each other. We will here make this more precise and derive some important consequences. In Sec. II E we argue that the density in any flowing region is essentially constant, and thus mass conservation ensures that the flow is divergence free. This will be assumed already here.

Consider a system for which it is possible to find a reference frame such that the velocity field is time independent (e.g., in the center of mass frame). We define a flow sheet as a surface in the flow, such that if a material point starts out on the surface, it stays on the surface throughout the time evolution of the system. If there are no strains within the sheet, we will refer to it as shear-free sheet (SFS). That is to say that the restriction of the strain-rate tensor to the sheet vanishes. The flows treated later are such that the whole shearing region can be divided into a collection of SFSs (the SFSs form a foliation of space occupied by the shear band). In any orthogonal and normalized basis field, with the two first basis vectors tangential to the SFS, the component form of the strain tensor is

$$(\underline{\underline{D}}) = \begin{pmatrix} 0 & 0 & d_1 \\ 0 & 0 & d_2 \\ d_1 & d_2 & 0 \end{pmatrix}. \tag{5}$$

Here we have used the fact that the total flow is assumed to be divergence free, $\nabla \cdot \underline{v} = \mathrm{tr}\, \underline{\underline{D}} = 0$. Hence, the principal-strain rates are $\gamma_1 = 0$ and $\gamma_{2,3} = \pm\sqrt{d_1^2 + d_2^2}$. The major advantage of considering these flows is now obvious: The ratio between the principal-strain rates remain constant throughout the system (even though d_1 and d_2 are free to vary). Thus we can drop this dependence in stress tensor, giving

$$\underline{\underline{\sigma}}_0 = \underline{\underline{\sigma}}_0(\theta_i, \dots). \tag{6}$$

The strain-rate ratios will be dropped from now on, and the ability to do so is crucial for the rest of the development. This enables us to probe the angle dependence alone. By a simple rotation in the SFS, the component form of the strain-rate tensor can be recast as

$$(\underline{\underline{D}})_{\mathrm{SFS}} = \begin{pmatrix} 0 & 0 & 0 \\ 0 & 0 & \dot{\gamma} \\ 0 & \dot{\gamma} & 0 \end{pmatrix}, \quad \dot{\gamma} = \sqrt{d_1^2 + d_2^2}. \tag{7}$$

We will refer to the basis that realizes this component form of the strain-rate tensor as the SFS basis, $\{\underline{e}_1, \underline{e}_2, \underline{e}_3\}$. Viscometric flows [28] have this form of the strain-rate tensor, but since we will put much emphasis on the physical picture offered by the SFS, we will continue to refer to these flows as SFS flows. This simple form tells us that the shear between planes is always directed along $\underline{e}_2$. Hence, for these flows we have a picture consistent with the SFSs sliding past each other (see Fig. 2). For later reference the principal-strain basis (the basis spanned by the eigenvectors of $\underline{\underline{D}}$) $\{\underline{p}_1, \underline{p}_2, \underline{p}_3\}$ is easily seen to be given as

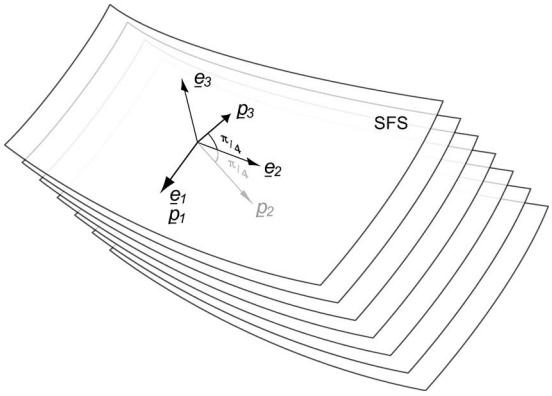

FIG. 2. Pictorial view of the partitioning of space into a set of SFS. Also illustrated is a specific instance of the SFS basis, and the corresponding principal-strain basis.

$$\underline{p}_1 = \underline{e}_1, \quad \underline{p}_{2,3} = (\underline{e}_2 \mp \underline{e}_3)/\sqrt{2}, \tag{8}$$

in terms of the SFS basis (see Fig. 2). We now proceed to argue for a specific form of the stress tensor in these two bases.

C. Stress relaxation

We claim that in the principal-strain basis the stress tensor takes the form

$$(\underline{\underline{\sigma}}_0)_{\mathrm{P}} = \begin{pmatrix} P^1 & 0 & 0 \\ 0 & P^2 & 0 \\ 0 & 0 & P^3 \end{pmatrix}, \quad P^i = P^i(\theta_j, \ldots). \tag{9}$$

To justify this we argue that force fluctuations are rapid in shearing flows. At any instance, two neighboring fluid elements, positioned relative to each other along any of the principal-strain directions, perform only a collective rigid body, and a relative stretching movement. Since these material points are not shearing, no shear forces should be generated between them. If any such forces are present as the material points enter this no-shear configuration, we assume that they relax fast enough to be ignored. The assumption that the principal directions of strain and stress are aligned is also central to the flow rules for many of the existing continuum models of granular flow (see Ref. [1] and references therein). In the SFS basis the stress tensor takes the form

$$(\underline{\underline{\sigma}}_0)_{\mathrm{SFS}} = \begin{pmatrix} P' & 0 & 0 \\ 0 & P & \tau \\ 0 & \tau & P \end{pmatrix}, \quad \begin{aligned} P' &= P^1 \\ P &= \tfrac{1}{2}(P^2 + P^3) \\ \tau &= \tfrac{1}{2}(P^2 - P^3), \end{aligned} \tag{10}$$

which again makes the connection to solid friction between the SFSs. So, the introduction of the SFS enables us to construct a physically relevant analogy with solid friction, which, as will be shown below, yields testable predictions. This is crucial for what remains.

D. The continuity equation

Mass conservation, and the fact that we assume the packing fraction to be constant throughout the shearing region, implies that the velocity field is divergence free. The linear-momentum continuity equation, in conjunction with angular-momentum continuity (and the requirement that there is no torque body couple), ensures that the stress tensor is symmetric, $\underline{\underline{\sigma}} = \underline{\underline{\sigma}}^{\dagger}$. This is something we have already implicitly assumed above. The linear momentum continuity equation reads

$$\frac{d(\rho \underline{v})}{dt} + \underline{\nabla} \cdot \underline{\underline{\Pi}} = \underline{F}, \tag{11}$$

where $\underline{F}$ is the body force, and the momentum-flux tensor is defined as $\underline{\underline{\Pi}} = \rho \underline{v}\underline{v} + \underline{\underline{\sigma}}$. As we are interested in quasistatic flows, we will neglect the $O(|\underline{v}|^2)$ term in the definition of the momentum-flux tensor. We will further only be interested in steady flows, and under these conditions the continuity equation for linear momentum takes the form of a force balance equation

$$\underline{\nabla} \cdot \underline{\underline{\sigma}} = \underline{F}. \tag{12}$$

The number of additional equations needed to close such a system is dependent on the symmetries present, and will be addressed for the four geometries considered below. We now turn to dimensional analysis to determine what the relevant dimensionless parameters are.

E. Dimensional analysis and additional assumptions

Obvious local parameters for the flow are the volume fraction ϕ, the material density ρ_{m}, the different local stresses in the SFS basis, the particle diameter a, and the shear rate $\dot{\gamma}$. There is a further possibility that the local bulk force influences the shear stress differently depending on how it is oriented with respect to the SFSs. If this is the case we must retain a dependence of the stress tensor on the orientation of the principal-strain basis with respect to the bulk force. This is encoded in the angles θ_i, and since there is a one-to-one correspondence between the principal-strain basis and the SFS basis we can take these angle to be defined with respect to the latter instead of the former. We can now form the dimensionless quantities

$$\phi, \mu = \tau/P, \quad \nu = P'/P, \quad \theta_1, \theta_2, \theta_3, \tag{13}$$

as the shear rate is taken to zero. Since the grains are hard we assume the packing fraction to be independent of the pressure ratios, as well as the angles. Hence, we take the packing fraction to be constant through the quasistatic regime, and we drop it from the development. Experimental and numerical justifications for this are referred to in Sec. IV. The only dimensionless quantity that can be constructed with the strain rate is

$$I = \frac{\dot{\gamma} a}{\sqrt{P/\rho_{\mathrm{m}}}}. \tag{14}$$

It was shown in Ref. [11] that I is the essential parameter determining how the material flows. Quasistatic flow is to be expected for I of order 10^{-3} or less.

As an aside we mention that for a general I in a SFS system (we assume $\dot{\gamma} > 0$ for simplicity) we can write

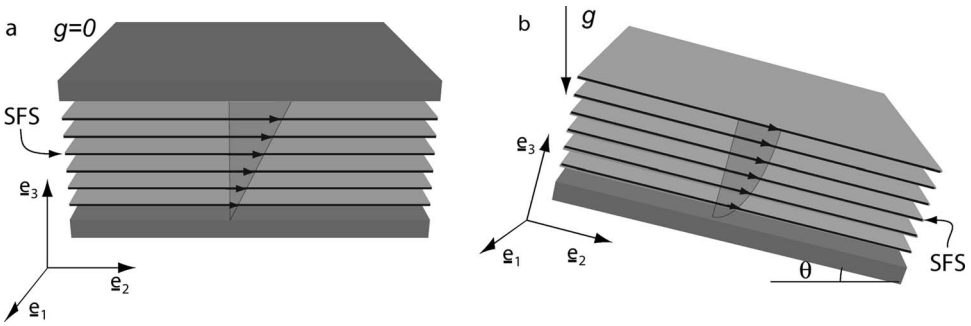

FIG. 3. The plane shear cell, and the inclined plane geometry, with the SFS as well as the SFS bases indicated.

$$\underline{\underline{\sigma}}_1 = \underline{\underline{\sigma}} - \underline{\underline{\sigma}}_0 = \Delta P' \underline{\underline{I}} + \Delta\tau(\underline{\underline{D}}/\dot{\gamma}) + \Delta P(\underline{\underline{D}}/\dot{\gamma})^2, \quad (15)$$

where the second equality defines the coefficients $\Delta P'$, ΔP, and $\Delta\tau$ through (1). It is also clear that the coefficients all must vanish for vanishing shear rates. For a SFS system only one of the fundamental invariants is nonzero,

$$I_D = 0, \quad II_D = \dot{\gamma}^2, \quad III_D = 0, \quad (16)$$

and we have

$$\underline{\underline{\sigma}}_1 = \begin{pmatrix} \Delta P'(\dot{\gamma}) & 0 & 0 \\ 0 & \Delta P(\dot{\gamma}) & \Delta\tau(\dot{\gamma}) \\ 0 & \Delta\tau(\dot{\gamma}) & \Delta P(\dot{\gamma}) \end{pmatrix}. \quad (17)$$

Hence we conclude that the general form of the stress tensor is preserved even for finite shear rates. These predictions should all be possible to check by simulating these systems. The above forms should also be useful when considering the stability of these flows, and the velocity field on the SFSs. Neither are investigated further in the present paper. Instead we continue to focus on the SFS in the quasistatic regime.

Returning to the rate independent case, and in analogy with solid friction, we make the additional assumption that the in-plane pressures of SFSs do not affect the friction between the SFSs. Thus we assume μ and ν to be independent. That is, the equation of state, relating all the dimensionless parameters, splits into two separate equations

$$\mu = \mu(\theta_i), \quad \nu = \nu(\theta_i), \quad (18)$$

where the actual forms depend on the material. We therefore have four independent quantities, say P, θ_1, θ_2, and θ_3, over a three-dimensional space.

Alternatively, if we had the full velocity field of some suitable system, say through numerical simulations, we could calculate the principal-strain basis and check that the stress tensor has the appropriate form (9). If this turns out to be true, we can gain information about the setup-dependent functions μ and ν by comparing the stresses.

III. FLOWS WITH WIDE SHEAR ZONES

The four systems we consider (see Fig. 1) all display wide shear zones and are also easily identified as SFS flows. We start by considering two systems with a high degree of symmetry, and then move on to the rather nontrivial split-bottom Couette geometries.

A. Planar shear, and inclined plane geometries

The first two geometries, to which we apply the above, are those of the linear shear cell without a gravitational field, and the inclined plane in a gravitational field (see Fig. 3). Due to the symmetry present in both geometries, we can directly identify the SFS as being parallel to the boundaries. Hence, $\underline{e}_3$ is always perpendicular to these. The only shear present between the planes is in the direction of the velocity, so $\underline{e}_2$ points in the flow direction, and $\underline{e}_1 = \underline{e}_2 \wedge \underline{e}_3$. The strain-rate tensor has the expected form (7) with $\dot{\gamma} = dv/dx^3$. In the considered geometries the principal-strain directions are constant throughout the sample, and thus the angles θ_i are also constant.

The plane-shear geometry is trivial in that all the elements of the SFS basis constitute a bulk symmetry direction. Hence, all relevant parameters must be constant throughout the bulk. Symmetry alone has already fixed the SFS planes, and appealing to subdominant dependence on I, we conclude that the shear rate is constant. This gives a linear velocity profile under the assumption that the boundaries do not break the symmetry by inducing localization of the shear zone.

In the inclined-plane geometry the $\underline{e}_3$ direction is no longer a bulk symmetry direction, and thus I is not constant along $\underline{e}_3$. Hence we have a more complicated velocity profile. From equation (12), or by simple force balance arguments between the SFSs, we have $\mu = \tan\theta$ (where θ is introduced in Fig. 3). Since the requirement on the effective-friction coefficient to be constant is geometrical in origin, it holds true to all orders in I. Including a subdominant dependence on I in the effective-friction coefficient, $\mu = \mu(\theta, I) = \tan\theta$, thus tells us that I is constant throughout the sample. This gives the well-known Bagnold profile [11,17,34].

Further, in this system the numerical results of Ref. [17] (the small inclination setups in three dimensions) show a linear relation between the pressures. It is also seen that the pressures σ_{22} and σ_{33} are very close to equal, while σ_{11} differs substantially from the others. In the above treatment we have $\sigma_{22} = \sigma_{33} = P$, in agreement with the numerical findings.

In both of the above cases we have argued that the actual velocity profiles are set by the subdominant dependence on the shear rate. If true, we would expect strong fluctuations of the velocity around the average profile, something observed in both systems described above [11,35].

B. Modified Couette geometry

In both of the linear geometries considered above, predicting the shape of shear zones in terms of SFSs is trivial

since symmetry guarantees that the SFSs are parallel with the boundaries. Balancing the stresses is hence also trivial due to the special form of the stress tensor in the SFS basis. We now tackle the modified Couette geometry. Compared with the examples considered so far, this system has lost the symmetry in the $\underline{e}_1$ direction (along the SFS perpendicular to the shear; see Fig. 1). The remaining symmetry in the $\underline{e}_2$ direction is either rotational, as in the case of the modified Couette system [Fig. 1(c)], or translational as in the linear system [Fig. 1(d)]. Though the loss of symmetry makes the treatment much more involved, it will lead to the conclusion that a constant effective-friction coefficient is *not* consistent with slow granular flows in general—we will find that the appropriate shape of SFS that describes the expected wide shear zones does not occur when we have a constant effective friction coefficient. We suggest that a dependence of the friction on the local angles, as indicated in Eq. (18), is crucial to understand such slow granular flows.

1. Rotational symmetry along the shearing direction

The system depicted in Fig. 1(c) consists of a cylindrical container filled with a granular material, and with a split-bottom plate. The inner part of the container is rotated at an angular velocity Ω, long enough for a steady state to be reached. The key experimental finding regards the spread of a wide shear band from the bottom slit up through the bulk to the surface. Naturally most data was collected for the velocity profiles at the top surface, as a function of the total height of the sample H.

It was found in Refs. [18,19] that the center position of the shear zone, R_c, and its width, W, satisfy simple scaling relations as function of the layer height, H, the radial position of the bottom slit, R_s, and the grain diameter, a. To good accuracy

$$1 - R_c/R_s = (H/R_s)^{5/2},$$

$$W \propto H^{2/3} a^{1/3}. \tag{19}$$

Though the experiments naturally focused on the velocity profiles at the top surface, there is also evidence that inside the bulk, away from the surface, the width of the shear zone scales with the height above the bottom z as $W(z) \propto z^{\alpha}$, with α somewhere between 0.2 and 0.4. [19,20,36].

In the natural cylindrical coordinate system, with the normalized basis $\{\underline{e}_r, \underline{e}_\varphi, \underline{e}_z\}$, we have $\underline{v} = v\underline{e}_\varphi$, and thus

$$(\underline{\underline{D}})_{\mathrm{cyl}} = \frac{r}{2}\begin{pmatrix} 0 & \partial_r\omega & 0 \\ \partial_r\omega & 0 & \partial_z\omega \\ 0 & \partial_z\omega & 0 \end{pmatrix}, \quad \omega = v/r. \tag{20}$$

Due to the symmetry of the problem, the surfaces of constant angular velocity are identified as the SFSs. By choosing the SFS basis

$$\underline{e}_1 = \frac{1}{|\underline{\nabla}\omega|}(\partial_z\omega\underline{e}_r - \partial_r\omega\underline{e}_z),$$

$$\underline{e}_2 = \underline{e}_\varphi,$$

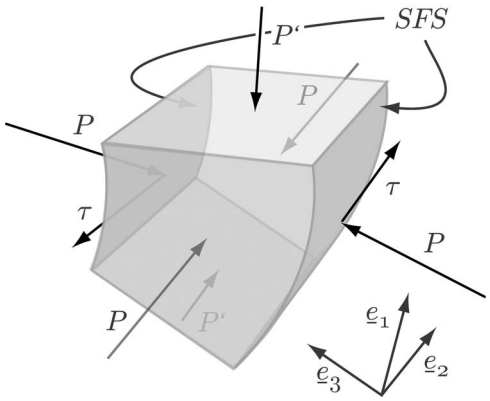

FIG. 4. Forces acting on a small element of material sandwiched between two shear-free sheets (indicated).

$$\underline{e}_3 = \frac{1}{|\underline{\nabla}\omega|}(\partial_r\omega\underline{e}_r + \partial_z\omega\underline{e}_z), \tag{21}$$

we arrive at the right form of the strain-rate tensor (7), with $\dot{\gamma} = r|\underline{\nabla}\omega|/2$. Due to the complicated geometry we need to work with the full momentum-continuity equations (12) in order to proceed. We denote the derivative along the $\hat{e}_i$:th direction as $d/dx^i := \hat{e}_i \cdot \underline{\nabla}$. In Fig. 4 we have sketched a local cuboidal element of material contained between two SFSs and illustrate the forces a stress tensor of the form Eq. (10) would give rise to.

We introduce the angle θ as the angle that $\underline{e}_1$ makes with the z axis, $\kappa_1 = d\theta/dx^1$ as the curvature of the integral curves of $\underline{e}_1$ (constant-ω curves), and $\kappa_3 = d\theta/dx^3$ as the curvature of the integral curves of $\underline{e}_3$. Taking care of the fact that the SFS basis forms the normalized basis vectors of a curved coordinate system, and using the machinery of tensor algebra, we can write Eq. (12) in the SFS basis as

$$\frac{dP'}{dx^1} + (P - P')(\kappa_3 - \sin\theta/r) = -\rho g \cos\theta,$$

$$\frac{d\tau}{dx^3} + (\kappa_1 - 2\cos\theta/r)\tau = 0,$$

$$\frac{dP}{dx^3} + (P - P')\kappa_1 = -\rho g \sin\theta. \tag{22}$$

In the modified Couette setup depicted in Fig. 1(c), we only need to specify θ to fix the SFS basis. Hence the relations between stress components and angles become of the form

$$\tau = \mu(\theta)P, \quad P' = \nu(\theta)P. \tag{23}$$

The full equations (22) coupled to Eq. (23) are too complicated for a full analytical treatment. We therefore will start from the simple assumption that the normal stress ratio ν is equal to 1 (i.e., $P' = P$), and that μ is constant, i.e., independent of θ. Then we are left with the equations

$$\frac{dP}{dx^1} = -\rho g \cos\theta,$$

$$\frac{dP}{dx^3} + (\kappa_1 - 2\cos\theta/r)P = 0,$$

$$\frac{dP}{dx^3} = -\rho g \sin\theta. \tag{24}$$

The curvature κ_3 has dropped out, and the first and last equations can be integrated to give a hydrostatic pressure profile $P=\rho g(H-z)$. Upon substituting this into the second equation we conclude that the curvature of the constant-ω curves satisfies,

$$\kappa_1 = \frac{2\cos\theta}{r} + \frac{\sin\theta}{H-z}. \tag{25}$$

To connect this formalism to the actual shapes of the SFS, let $r(z)$ be the curves of constant ω. Using that $dr/dz=\tan\theta$ it follows that

$$\sin\theta = \frac{r'(z)}{\sqrt{1+[r'(z)]^2}}, \quad \cos\theta = \frac{1}{\sqrt{1+[r'(z)]^2}},$$

$$\kappa_1 = \frac{r''(z)}{\{1+[r'(z)]^2\}^{3/2}}. \tag{26}$$

Hence using (25) and (26) we see that the curves of constant angular velocity must satisfy

$$r''(z) = \{1+[r'(z)]^2\}\left(\frac{2}{r} + \frac{r'(z)}{H-z}\right). \tag{27}$$

This is a second-order differential equation which can be solved numerically when supplemented with two boundary conditions. This turns out to be exactly the same differential equation one arrives at through minimizing the functional

$$f[r(\cdot)] = \int_0^H \mathrm{d}z(H-z)r^2(z)\sqrt{1+[r'(z)]^2}. \tag{28}$$

As was shown by Unger and co-workers [24], this functional can be seen to describe the torque needed to shear an ideal cohesionless Coulomb material under hydrostatic pressure which has its infinitesimal shear zone at $r(z)$. Minimizing this torque, a definite prediction for $r(z)$ was obtained which qualitatively captures the shear zone location as measured experimentally. We refer to Refs. [19,20,24] for further discussion.

However, this approach cannot result in shear zones with a width of the form seen in experiments, $W(z)\propto z^\alpha$, with $0.2<\alpha<0.5$. To see this, one only has to consider the profiles close to the bottom. We now assume that a general level curve has the form [37]

$$r_1(z) = r_0(z) + Az^\alpha + \text{h.o.t.}, \tag{29}$$

where $r_0(z)$ is the center curve, and A some constant specifying the specific level curve under consideration. Upon substituting this into Eq. (27), and considering the lowest order in z, we conclude that α equals 0 or 1. This contradicts the experimental findings.

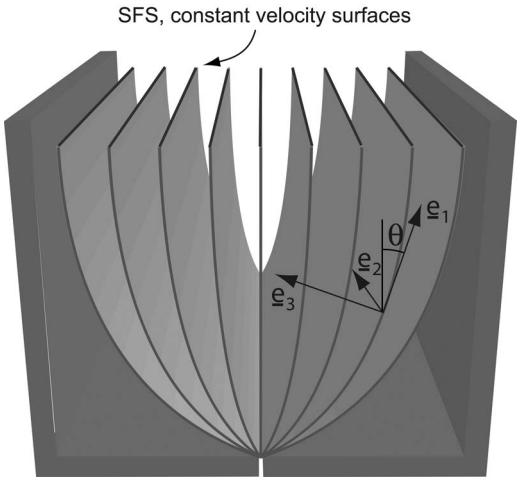

FIG. 5. Schematic cross section of the linear modified Couette geometry with the expected form of the SFSs indicated.

From this we conclude that our assumptions that ν and μ are constant are not consistent with the wide shear zones observed in the modified Couette geometry.

This curved geometry is, however, too complicated to study the precise role of more general ν and μ. We will therefore turn our attention to the closely related linear split-bottom shear cell, which can be obtained by letting the slit radius diverge, and where the rotational symmetry in the $\underline{e}_2$ direction is replaced by a simpler translational symmetry.

2. Translation symmetry along the shearing direction

The scaling forms (19) relate the shear zones width W, and location R_c, to the particle size a, height H, and radius of curvature of the slit R_s. Taking the limit $R_s\to\infty$ enables us to estimate what flow profiles can be expected in the linear setup shown in Fig. 1(d), even though no experimental or numerical data is available for such a system at present [38]. The width is independent of R_s, while the shift between R_s and R_c should vanish in this limit. We therefore expect qualitatively the same widening of the shear zone as in the Couette geometry [Fig. 1(c)], with the shear zones center remaining straight above the linear slit (consistent with the reflection symmetry of such a linear geometry), as indicated in Fig. 5.

The equations for linear momentum conservation simplify to

$$\frac{dP'}{dx^1} + (P-P')\kappa_3 = -\rho g\cos\theta,$$

$$\frac{d\tau}{dx^3} + \kappa_1\tau = 0,$$

$$\frac{dP}{dx^3} + (P-P')\kappa_1 = -\rho g\sin\theta. \tag{30}$$

Let us for the moment assume that μ is a constant, and test whether this assumption is consistent with the flow profiles sketched in Fig. 5. For constant-friction coefficient, the

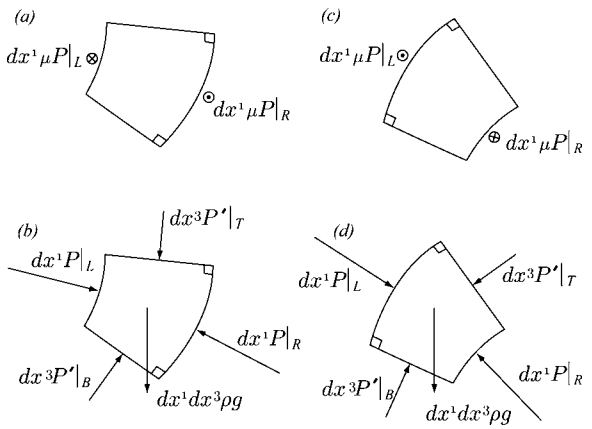

FIG. 6. Illustration of the simple force balance arguments which shows that a constant μ is incompatible with an upward bending edge of the shear zone. For details, see text.

last two equations above can be combined to give

$$P'\kappa_1 = \rho g \sin\theta. \tag{31}$$

For profiles that bend upward when going through the bulk (see Fig. 5), κ_1 and θ are of opposite signs. Hence, to satisfy Eq. (31), P' has to be negative, which is impossible in cohesionless granular materials.

Thus we have two possible scenarios: If the effective friction coefficient is constant, then the system cannot support a wide shear zone, and the shear must localize. Considering that the cylindrical geometry exhibits a width of the shear zone that is apparently independent of the position of the bottom slit, it seems more likely, though, to have the upward bending profiles also in the linear geometry. Hence, the effective friction coefficient must decrease as we move away from the center, along the integral lines of $\underline{e}_3$. This is a strong statement since it does not rely on assuming any specific form for ν, the ratio between the normal pressures: Even with normal stress differences we cannot get a qualitatively correct description assuming the effective-friction coefficient to be constant throughout the bulk.

The same conclusion can be reached by considering force balance on a cuboid element of material contained between two SFSs as illustrated in Figs. 6(a) and 6(b), and employing the special form of the stress tensor in the SFS basis (10). We start from the fact that the total shear forces $dx^1dx^2\mu P$ acting on the left and right edges of the cuboid need to balance. Now if μ is a constant this implies that the normal forces on left and right of the cuboid equal: $dx^1dx^2P|_L = dx^1dx^2P|_R$ [Fig. 6(a)]. The only additional forces acting on the cuboid are gravity ($dx^1dx^2dx^3\rho g$) and the normal forces on top and bottom of the cuboid $dx^2dx^3P'|_{T,B}$ [Fig. 6(b)]. Due to the upward bending of the SFSs, the sum of these three terms clearly has a substantial component towards the right—hence it is impossible to balance forces in the $\underline{e}_3$ direction in this case. For "outward" bending SFS this problems does not occur as illustrated in Figs. 6(c) and 6(d).

In our case, the only way to attain force balance is if the normal force acting on the right face of the cuboid is larger than the force acting from the left: $dx^1dx^2P'|_L < dx^1dx^2P'|_R$. Since the shear forces still have to balance, this is only possible when μ is not a constant—in fact μ has to reach its *maximum* along vertical SFSs and then gradually decrease as we move outward towards increasingly slanted SFSs (along the $\underline{e}_3$ direction).

The next step is thus to include a θ dependence in the effective-friction coefficient and see if this is sufficient to be able to obtain shear zones of finite width. For simplicity, we keep $\nu(\theta)=1$. As before, two of the momentum continuity equations can be solved and yield a hydrostatic pressure profile, $P=\rho g(H-z)$. The third momentum continuity equation becomes

$$\frac{d\ln\mu(\theta)}{dx^3} + \frac{d\theta}{dx^1} = \frac{\sin\theta}{H-z}. \tag{32}$$

To get an analytically tractable problem we now consider a region close to the central level curve $r(z)=0$. Since odd powers of θ can be excluded due to the $\theta\to-\theta$ symmetry, we assume that we can expand the friction coefficient as

$$\mu(\theta) = \mu_0\left(1 - \frac{1}{2}q\theta^2\right) + O(\theta^4). \tag{33}$$

Sufficiently close to the central level curve θ is small, and we can, to lowest order, rewrite the derivatives d/dx^1 and d/dx^3 as $\theta\partial_r+\partial_z$ and $-\partial_r$ respectively. Hence the momentum conservation equation (32) can be rewritten, to lowest order, as

$$(1+q)\theta\frac{\partial\theta}{\partial r} + \frac{\partial\theta}{\partial z} = \frac{\theta}{H-z} + \text{h.o.t.} \tag{34}$$

This differential equation can be solved by the method of characteristics, resulting in

$$\theta(r,z) = -\frac{r/H}{(1+q)(1-z/H)\ln(1-z/H)} + \text{h.o.t.} \tag{35}$$

Close to the bottom where $z/H \ll 1$, we expect the constant-ω lines to satisfy $r(z)\propto z^\alpha$, with an exponent α somewhere between 0.2 and 0.5 [19]. In this limit, (35) can be integrated using the fact that for any level curve we have $r'(z) = \tan\theta[r(z),z]$. This results in

$$r(z) \propto z^{1/(1+q)}, \quad z/H, \theta \ll 1. \tag{36}$$

The result of numerically integrating the full form given in Eq. (35) is shown in Fig. 7. The only sensible profiles are achieved for $q>0$. This is in agreement with the arguments sketched in Fig. 7, indicating that upward bending constant-ω lines are possible only if μ decreases with increasing $|\theta|$. Hence, the highest effective-friction coefficient is achieved when the direction of gravity lies in the tangent plane of the shearing surfaces [39].

IV. DISCUSSION AND CONCLUSION

To address the question of whether continuum models can be made consistent with experimental and numerical observations of wide shear zones in slow granular flows, we have made a number of assumptions, which we will briefly recapitulate here. Trivially, we assume that the flow profile is

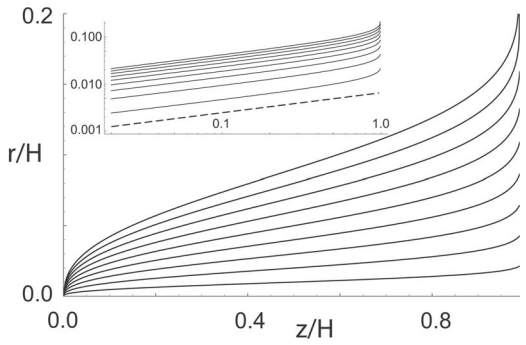

FIG. 7. Plots of the constant-ω lines as calculated numerically in the small θ approximations (33) for $q=1.5$, giving an exponent $\alpha = 1/(1+q)=0.4$ close to the bottom. The inserted graph depicts the same curves on a log-log scale, and with the 0.4 power indicated by the dashed line.

smooth on a coarse-grained scale. Furthermore we assume local action (see Sec. II) and material objectivity (see Sec. II), and focus on steady states for which the shearing direction is a symmetry direction of the system—this washes out memory effects (see Sec. II). The considered flows are sufficiently symmetric, and time independent, so that they can be described by time-independent shear-free sheets. All these assumptions appear rather inconspicuous.

But there are a number of less obvious assumptions which deserve more attention, and for which a numerical test would be extremely useful. The first of these is the absence of elastic shear stresses in the flowing zone, due to rapid (on a macroscopic time scale) relaxation of force fluctuations (see Sec. II C). Clearly, in a large system, far away from the shear zone, elastic stresses should play a role, but here we only consider the actual flowing region. It is an open question when and where such elastic stresses start to play a role. Second, we assume that the packing fraction is constant throughout the flowing region. Recent magnetic resonance imaging (MRI) measurements of the packing density suggest an approximately constant dilated region in the flowing zone [40]. Nevertheless, far away from the shear zone the density is observed to be different from this region. Finally we have excluded a possible dependence of the effective-friction coefficient on the pressure ratio, ν, within the SFS (see Sec. II E). This assumption lacks a strong physical argument but is made to keep the problem tractable, and should be an important issue to check numerically.

Using the assumptions recapitulated above, our method is based on separating out those parameters of the strain-rate tensor that are explicitly rate dependent. This enables us to build a explicitly rate-independent theory, and we have shown that it is able to predict some of the features of the stresses seen in numerical simulations of the inclined plane geometry, as well as capturing the widening of the shear zone in the modified Couette geometry.

Through the introduction of shear-free sheets we have also clarified when a direct interpretation along the lines of solid friction can be made, and further indicated how far such an analogy can be stretched. Due to that the flow could be considered as consisting of SFSs, no special assumptions had to be made regarding the effect of a variation in the principal-strain rate ratios throughout the sample. It was further shown that in order to account for the expected shape of the shear zones, the proportionality constants between the different pressures (e.g., the effective-friction coefficient) must retain a dependence on the local orientation of the flow (i.e., the orientation of the principal-strain basis) relative to the local body force—the only other probable alternative is that the shear zone is not wide. We speculate that the origin of such angle dependence is due to the competition between the organizational tendencies of the flow and the gravitational pull. The flow tends to increase the number of grain contacts in compressional directions, while decreasing the number in expanding directions. At the same time, the gravitational pull leads to an increased number of vertical, opposed to horizontal, connections (rattlers always fall down). Unfortunately, however, not enough is known about such angle dependence of the contact network in order to confirm our speculations. We suggest that this angle dependence as an important issue for future research.

Due to the explicit rate independence of the approach, it cannot give the complete velocity profile. In order to determine the complete profile one needs to include the subdominant rate dependence in the stress tensor. This is straightforward for some simple geometries and should be possible in general. Unfortunately it turns out to be nontrivial even for the relatively simple modified Couette geometry.

Nevertheless, the intriguing fact that the experimental shear profiles in this geometry fitted an error function so well provides an important benchmark for understanding quasistatic flow. As we have discussed in Sec. III B 2, a linear version of this experiment may provide important additional information.

The present approach poses a set of well-defined questions regarding the packing fraction in the shear zone, the linear relationship between pressures, the simple form of the stress tensor in the SFS basis, and the dependence of the proportionality stress ratios μ and ν, on the orientation of the shear planes with respect to gravity. These are simple basic issues which are open to investigation by numerical simulations, and possibly even by experiments. Clarifying these issues appears crucial for further development of a theory along these lines.

ACKNOWLEDGMENTS

We gratefully acknowledge illuminating discussions with Ellák Somfai, Hans van Leeuwen, Wouter Ellenboek, and Alexander Morozov. M.D. acknowledges financial support from the physics foundation FOM and PHYNECS, and M.vH. acknowledges financial support from the science foundation NWO through a VIDI grant.

[1] R. Jackson, J. Rheol. **30**, 907 (1986).
[2] J. T. Jenkins and S. B. Savage, J. Fluid Mech. **130**, 186 (1983).
[3] P. K. Haft, J. Fluid Mech. **134**, 401 (1983).
[4] C. S. Campbell, Annu. Rev. Fluid Mech. **22**, 57 (1990).
[5] I. Goldhirsch, Chaos **9**, 659 (1999).
[6] C. Bizon, M. D. Shattuck, J. B. Swift, and H. L. Swinney, Phys. Rev. E **60**, 4340 (1999).
[7] R. M. Nedderman, *Statics and Kinematics of Granular Materials* (Cambridge University Press, Cambridge, England, 1992).
[8] L. Bocquet, W. Losert, D. Schalk, T. C. Lubensky, and J. P. Gollub, Phys. Rev. E **65**, 011307 (2001).
[9] C. T. Veje, D. W. Howell, and R. P. Behringer, Phys. Rev. E **59**, 739 (1999).
[10] S. Douady, B. Andreotti, and A. Daerr, Eur. Phys. J. B **11**, 131 (1999).
[11] GDR MiDi, Eur. Phys. J. E **14**, 341 (2004), and references therein.
[12] M. Babic, H. H. Shen, and H. T. Shen, J. Fluid Mech. **219**, 81 (1990).
[13] P. A. Thompson and G. S. Grest, Phys. Rev. Lett. **67**, 1751 (1991).
[14] Y. Zhang and C. S. Campbell, J. Fluid Mech. **237**, 541 (1992).
[15] O. J. Schwarz, Y. Horie, and M. Shearer, Phys. Rev. E **57**, 2053 (1998).
[16] E. Aharonov and D. Sparks, Phys. Rev. E **65**, 051302 (2002).
[17] L. E. Silbert, D. Ertas, G. S. Grest, T. C. Halsey, D. Levine, and S. Plimpton, Phys. Rev. E **64**, 051302 (2001).
[18] D. Fenistein and M. van Hecke, Nature **425**, 256 (2003).
[19] D. Fenistein, J. W. van de Meent, and M. van Hecke, Phys. Rev. Lett. **92**, 094301 (2004).
[20] D. Fenistein, J.-W. van de Meent, and M. van Hecke, e-print cond-mat/0507442 (2005).
[21] *Jamming and Rehology*, edited by A. J. Liu and S. R. Nagel (Taylor & Francis, New York, 2001).
[22] T. S. Komatsu, S. Inagaki, N. Nakagawa, and S. Nasuno, Phys. Rev. Lett. **86**, 1757 (2001).
[23] D. Volfson, L. S. Tsimring, and I. S. Aranson, Phys. Rev. E **68**, 021301 (2003).
[24] T. Unger, J. Török, J. Kertész, and D. E. Wolf, Phys. Rev. Lett. **92**, 214301 (2004).
[25] R. Hartley and R. Behringer, Nature **421**, 928 (2003).
[26] E. Aharonov and D. Sparks, Phys. Rev. E **60**, 6890 (1999).
[27] B. Miller, C. O'Hern, and R. P. Behringer, Phys. Rev. Lett. **77**, 3110 (1996).
[28] G. Astarita and G. Marucci, *Principles of Non-Newtonian Fluid Mechanics* (McGraw-Hill, London, 1974).
[29] G. C. Phillipe, *Mathematical Elasticity* (Elsevier, Amsterdam, 1988).
[30] Nonlocal interactions would be possible if a macroscopic length scale is present in the bulk. This could happen for a system close to something reminiscent of a second-order phase transition. The existence of such a transition point, especially in the context of "jamming," where the mentioned critical point is often referred to as point *J*, is at present under active investigation [21,31–33]. The location of point *J* would be precisely at the packing fraction where the material starts to support an external shear load. The systems we hope to describe support finite shear stresses even as the shear rate approaches zero, and we are hence away from point *J*.
[31] A. J. Liu and S. R. Nagel, Nature **396**, 21 (1998).
[32] L. E. Silbert, A. J. Liu, and S. R. Nagel, Phys. Rev. Lett. **95**, 098301 (2005).
[33] C. S. O'Hern, L. E. Silbert, A. J. Liu, and S. R. Nagel, Phys. Rev. E **68**, 011306 (2003).
[34] R. A. Bagnold, Proc. R. Soc. London **A255**, 49 (1954).
[35] L. E. Silbert, Phys. Rev. Lett. **94**, 098002 (2005).
[36] X. Cheng, J. B. Lechman, A. Fernandez-Barbero, G. S. Grest, H. M. Jaeger, G. S. Karczmar, M. E. Möbius, and S. R. Nagel, Phys. Rev. Lett. **96**, 038001 (2006).
[37] Close to the bottom slit the system will no longer be quasistatic due to large gradients in the velocity field. On the other hand, this region can be made arbitrarily small by lowering the driving rate. Hence, a small-z expansion should have a finite region in which it accurately describes the behavior of the SFS.
[38] Preliminary experiments, performed in Leiden, in a conveyer belt geometry exhibit shear zones of finite width.
[39] Close to the top surface, as well as close to the bottom slit, the assumption of a small θ is no longer valid due to the (slow) divergence in Eq. (35), and the small z behavior of Eq. (36) respectively. On the other hand, we could never hope to describe these regions with a quasistatic theory due to that here I (as given in Sec. II E) becomes large, and we leave the quasistatic part of the flow.
[40] P. Umbanhowar, private communication.